

# Heightmap Reconstruction of Macula on Color Fundus Images Using Conditional Generative Adversarial Networks

Peyman Tahghighi\*, Reza A.Zoroofi\*, Sareh Saffi †, and Alireza Ramezani‡ §

\*School of Electrical and Computer Engineering

University of Tehran, Tehran, Iran

†Ophthalmic Research Center, Research Institute for Ophthalmology and Vision Science

Shahid Beheshti University of Medical Sciences, Tehran, Iran

‡Ophthalmic Epidemiology Research Center, Research Institute for Ophthalmology and Vision Science

Shahid Beheshti University of Medical Sciences, Tehran, Iran

§Negah Specialty Ophthalmic Research Center

Shahid Beheshti University of Medical Sciences, Tehran, Iran

Email: peyman.tahghighi@ut.ac.ir, zoroofi@ut.ac.ir, saresafi.s@gmail.com, arramezani@gmail.com

**Abstract**—For medical diagnosis based on retinal images, a clear understanding of 3D structure is often required but due to the 2D nature of images captured, we cannot infer that information. However, by utilizing 3D reconstruction methods, we can construct the 3D structure of the macula area on fundus images which can be helpful for diagnosis and screening of macular disorders. Recent approaches have used shading information for 3D reconstruction or heightmap prediction but their output was not accurate since they ignored the dependency between nearby pixels. Additionally, other methods were dependent on the availability of more than one image of the eye which is not available in practice. In this paper, we use conditional generative adversarial networks (cGANs) to generate images that contain height information of the macula area on a fundus image. Results using our dataset show a 0.6077 improvement in Structural Similarity Index (SSIM) and 0.071 improvements in Mean Squared Error (MSE) metric over Shape from Shading (SFS) method. Additionally, Qualitative studies also indicate that our method outperforms recent approaches.

## I. INTRODUCTION

Color fundus photography is a 2D imaging modality for the diagnosis of retinal diseases. 3D structure of the eye provides a considerable amount of crucial information for ophthalmologists to diagnose which is unavailable in 2D fundus images. Therefore, being able to infer this information from just a 2D image can be helpful. Furthermore, the reconstructed heightmap offers clinicians another means to view internal eye structure which may help them in better and more accurate diagnosis [1], [2]. Optical Coherence Tomography [3] is an expensive but vital tool for evaluating the retinal structure which provides ophthalmologists with valuable information, enabling them to diagnose most of the macular diseases. Nevertheless, owing to the cost of using this system, it is not ubiquitous and using fundus images is mostly common in clinics.

The only approach applied to this problem considering only one fundus image was Shape from Shading (SFS) [2] which

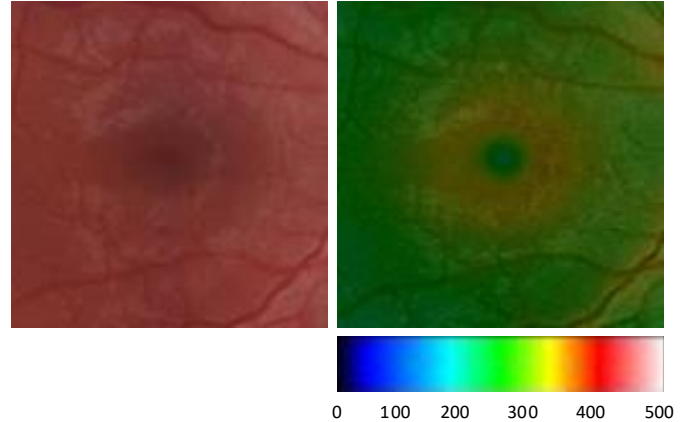


Fig. 1. The left and right image represent the correspondence between a fundus image and its heightmap image. As can be seen, each pixel's color value of the image on the right indicates a height according to color gradients below which ranges from  $0\mu\text{m}$  to  $500\mu\text{m}$ . Note that all numbers are in micrometer.

the result generated by this method was not accurate [1]. Additionally, others relied on two views of fundus image [4] which such data is not available since devices only take one image per eye.

Conditional generative adversarial networks (cGANs) [5] are a generative model that can generate images given a source image and enabled researchers to use this method for many image generation tasks [6], [7], [8], [9]. Considering Figure 1, since our problem can be seen as an image generation task in which we want to predict a color image containing heights data from the macula area on a fundus image, cGANs can be directly applied to this problem. That is to say, each pixel in the right image of Figure 1 has a color value which represents

a height from  $0\mu\text{m}$  to  $500\mu\text{m}$  and by predicting red, green and blue color values for each pixel of the left image, we can predict its heightmap. The color bar below Figure 1 shows the assignment of different color values to different heights.

For our generator, we used two blocks of connected U-Nets [10] which is called Cas-Net [6] and our discriminator network is an ImageGAN which classifies the whole image as real or fake. Furthermore, we used L2-Loss along with GAN loss and perceptual loss [11] to produce output. Even though using L2-Loss is less common in literature than L1-Loss, we decided to use it due to the benefit that it brought which will be discussed in section IV-G. Additionally, we specifically discuss the contribution of each of these loss functions in section IV-F.

To the best of our knowledge, this is the first research paper on predicting the heightmap of macula area on fundus images using deep neural networks (DNNs). We evaluated our approach qualitatively and quantitatively on our dataset and compared the results with the SFS method which showed an improvement in all measures.

## II. RELATED WORK

3D reconstruction has been well studied using multiple views that need at least two images to be able to 3D reconstruct the given image, including stereo based methods [12]. Another class of methods that can recover the 3D structure is called shape from shading which uses a gradual variation of shading of a single image to recover its 3D structure [13].

Considering heightmap prediction or 3D reconstruction of funduscopic images, Cherian *et al.* [2] used the aforementioned shape from shading method to recover the 3D structure of the macula area. Nonetheless, the final outcome of their approach was not accurate [1]. Additionally, Guo *et al.* [4] used disparity map estimation to 3D reconstruct the Optic-Nerve Head (ONH). However, their method is totally dependent on the presence of the left and right eye fundus images which is not available in practice.

Generative adversarial networks (GANs) [5] are an important approach for learning a generative model that can generate samples from real-world data distributions. A variation of this form of networks are conditional generative adversarial networks (cGANs) [14] in which the model is conditioned on external information such as an image. These methods consist of a generator and a discriminator in which the goal of the generator is to generate image according to the given input image and the role of the discriminator is to distinguish between real and generated images. Most recently, Isola *et al.* [8] proposed pix2pix-cGANs as a general solution to many problems which is dealing with image-to-image translation. In their work, instead of commonly used discriminators that classify each generated image into real or fake class, they proposed PatchGAN that can classify every patch of the image as real or fake which resulted in less blurry images [8]. Additionally, Johnson *et al.* [11] proposed perceptual loss which is the difference between the features extracted from different layers of the discriminator network for generated and ground-truth image and resulted in more detail in the final

output along with less blurriness [15], [16]. In their work, they used features extracted from pre-trained networks such as VGG [17]. However, Wang *et al.* [9] suggested using the features extracted from the discriminator itself since these external networks are trained on specific classification datasets such as ImageNet [18] and they mainly focus on features that contribute to that specific classification task and, as a result, may perform poorly on other unrelated tasks [9]. We also used the discriminator network for perceptual loss in our work.

Recently GANs have drawn attention in the medical field especially in the task of image-to-image translation. For instance, Wang *et al.* [19] suggested translating from artifact-corrupted scans to their artifact-free counterparts in CT scans of cochlear implants recipients. Armanious *et al.* [6] combined L1 loss with GAN loss and perceptual loss alongside style transfer loss on PET to CT translation, correction of MR motions and PET denoising. The role of style loss is to transfer the style of the input image (color, texture, common patterns, etc.) to output image [11]. In addition, they proposed a new generator architecture called CasNet which consists of six stacked U-Nets and with their method, they performed all three mentioned tasks with one single architecture and achieved state of the art results. We also adopted CasNet in our work as our generator network but with a different number of stacked U-Nets.

Finally, considering funduscopic images, Son *et al.* [20] used pix2pix-cGANs to segment the vessels of funduscopic images. Additionally, Iqbal *et al.* [21] proposed MI-GAN which can generate fundus images along with its ground-truth vessel segmentation and used its generated dataset to segment the vessels in a fundus image.

## III. METHOD

### A. Network structure

In our proposed cGAN setting, the input to our generator is a  $128 \times 128 \times 3$  image of the macula area on a fundus image and the generator will generate an image of the same size and depth which each pixel color indicates a height as depicted in Figure 1. The discriminator takes this image and gives a probability between 0 to 1 which indicates the similarity of this image to a real heightmap image.

Inspired by ResNets [22] which uses the information of the upper blocks in the lower blocks, in U-Net architecture [10], skip-connections are extensively used in form of concatenation to pass features from upper layers to lower layers as depicted in the first row of Figure 2. This helps us to avoid vanishing gradient problem which may happen especially in a deeper network like what we have here. All the blocks in U-Net have the form of Convolution-BatchNorm-LeakyReLU.

Our proposed generator consists of two stacked U-Nets. This is done such that the output of the first block is feed into the next block and this blocks' output is considered as the final output of the network. Therefore, the information passed between these blocks and their layers gradually refines and each layer can add its own level of detail to the final outcome [6]. Furthermore, although our network is deeper in

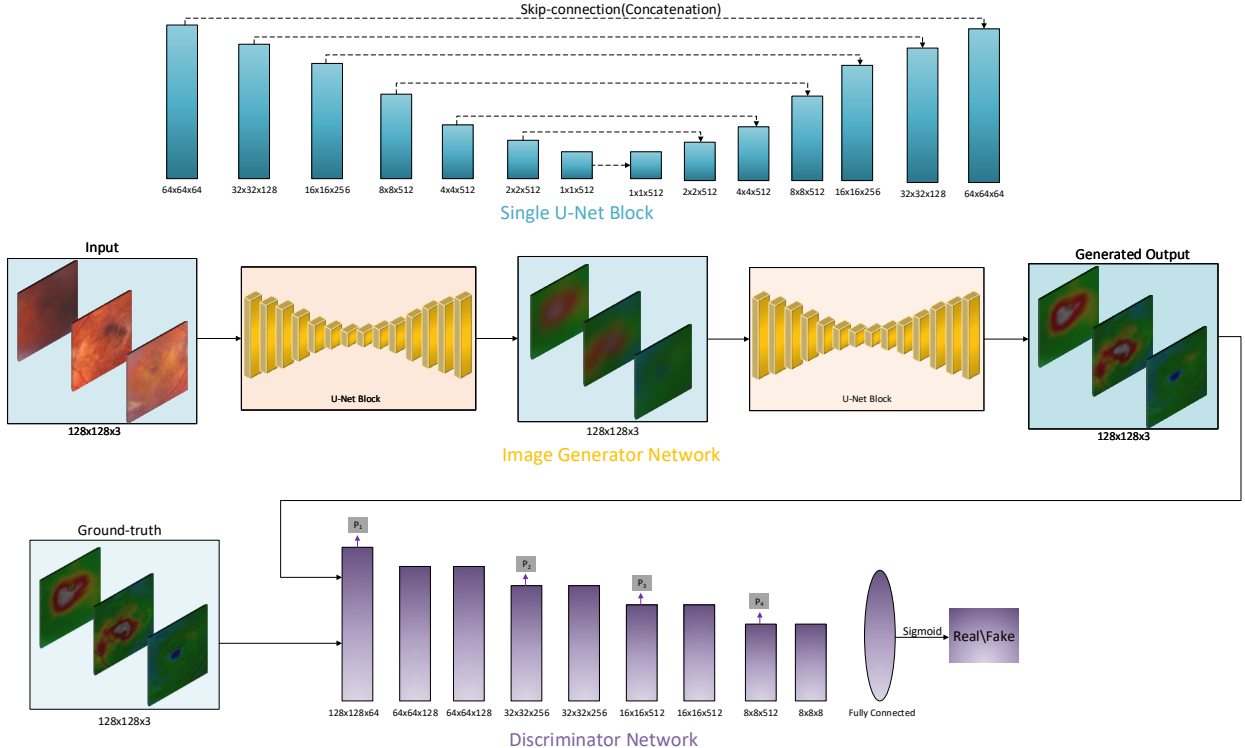


Fig. 2. Overview of the proposed deep learning system. It generally consists of a generator and a discriminator network. The image generator network is trained to synthesize heightmap images using given fundus images. In the first row, a single U-Net block is represented which is composed of a series of Convolution-BatchNorm-LeakyReLU encoding layers and Deconvolution-BatchNorm-ReLU decoding layers and skip-connections pass the information from upper layers (encoder layers) to lower layers (decoder layers). The generator in the second row is composed of 2 stacked U-Nets in which the image generated from the first layer is passed as input to the second layer and this layer outputs the final generated heightmap. The discriminator network in the third row also consists of Convolution-BatchNorm-LeakyReLU layers with a final fully connected layer. Additionally, four hidden layers as depicted in the third row are utilized to compute perceptual loss. The output of the network is in the form of probability and is used to distinguish between real and fake images.

comparison to a normal U-Net architecture, owing to skip-connections involved in the architecture, vanishing gradient problem will not happen and loss flows easily to upper layers through backpropagation because of skip-connections. This architecture is depicted in the second row of Figure 2.

Regarding discriminator, the judgment can be made at the image level as well as the patch level. That is to say, we can judge the quality of the entire image by our discriminator (ImageGAN) or consider its patches when we want to judge (PatchGAN). We explored both of these methods and opted for image level discriminator due to better quality images and higher values in all measures as discussed in Section IV-E. Similar to the generator network, each block in discriminator is in the form of Convolution-BatchNorm-LeakyReLU. Furthermore, As can be seen in the third row of the Figure 2, we used 1<sup>th</sup>, 4<sup>th</sup>, 6<sup>th</sup> and 8<sup>th</sup> layer of the discriminator network to compute perceptual loss between generated image and ground-truth image as a supervisory signal with the aim of better output. Finally, the last convolution layer is flattened and fed into a single sigmoid output to calculate the probability of the realness of the generated image.

### B. Objective functions

Our final loss function is composed of three parts which will be discussed in this section.

1) *Generative adversarial loss*: Let the generator  $G$  be a mapping from a fundus image  $x$  and a random noise vector  $z$  to a colored heightmap image  $y$ . Then, the discriminator  $D$  maps a pair of  $\{x, y\}$  to a probability between 0 and 1 where 0 means that the image is completely fake and 1 means that the image is completely real. Then, the objective function of conditional GAN can be formulated as :

$$L_{cGAN}(G, D) = \mathbb{E}_{x,y} [\log(D(x, y))] + \mathbb{E}_{x,z} [\log(1 - D(x, G(x, z)))] \quad (1)$$

Basically, conditional GAN can be regarded as a minimax game in which discriminator tries to maximize Equation 1, while generator tries to fool the discriminator and, as a result, minimize the value in Equation 1. Therefore, conditional GAN solves the optimization problem in Equation 2 :

$$\min_G \max_D L_{cGAN} \quad (2)$$

2) *Pixel reconstruction loss*: Image-to-image translation tasks that rely solely on the adversarial loss function do not produce consistent results [6]. Therefore, we also used pixel reconstruction loss here but we opted for L2-loss rather than widely used L1-loss since it performed better in reconstructing details in this specific task as discussed in IV-G. The Equation for L2-loss is as below:

$$L_{L2}(G) = \mathbb{E}_{x,y,z} [\| y - G(x, z) \|_2^2] \quad (3)$$

3) *Perceptual loss*: Despite producing plausible results using only two aforementioned loss functions, since the generated image is blurry [6] and especially in medical diagnosis small details are of significance, we used perceptual loss [9] to improve the final result. As a matter of fact, using only L2-Loss or L1-Loss results in outputs that maintain the global structure but it shows blurriness and distortions [9]. Furthermore, per-pixel losses fail to capture perceptual differences between input and ground-truth images. For instance, when we consider two identical images only shifted by some small offset from each other, per-pixel loss value may vary considerably between these two, even though they are quite similar [11]. However, by using high-level features extracted from layers of a discriminator, we can capture those discrepancies and can measure image similarity more robustly [11]. In our work, since discriminator network also has this capability of perceiving the content of images and difference between them and pre-trained networks on other tasks may perform poorly on other unrelated tasks, we used hidden layers of discriminator network [9], [6] to extract features as illustrated in the third row of the Figure 2. The mean absolute error for  $i^{th}$  hidden layer between the generated image and the ground-truth image is then calculated as :

$$P_i(G(x, z), y) = \frac{1}{w_i h_i d_i} \| D_i(x, y) - D_i(G(x, z), y) \|_1 \quad (4)$$

which  $w_i, h_i$  and  $d_i$  denote width, height and depth of the  $i^{th}$  hidden layer respectively and  $D_i$  means the output of  $i^{th}$  layer of the discriminator network. Finally perceptual loss can be formulated as :

$$L_{perceptual} = \sum_{i=0}^L \lambda_i P_i(G(x, z), y) \quad (5)$$

Where  $\lambda_i$  in equation 5 tunes the contribution of  $i^{th}$  utilized hidden layer on the final loss.

Finally our completed loss function for generator is as below:

$$L = \alpha_1 L_{perceptual} + \alpha_2 L_{L2} + \alpha_3 L_{cGAN} \quad (6)$$

where  $\alpha_1$ ,  $\alpha_2$  and  $\alpha_3$  are the hyperparameters that balance the contribution of each of different losses. It is noteworthy that we also used perceptual loss in training discriminator beside traditional cGAN loss with equal contribution.

## IV. EXPERIMENTS

### A. Dataset

The data was gathered from TopCon DRI OCT Triton captured at Negah Eye Hospital. First, we cropped the macula part of the fundus and heightmap image of the 3D macula report generated by the device to create image pairs. Then, we resized both images to 128x128 and normalized them to [0, 1] before feeding them into our network. Our dataset contains 3407 color fundus-heightmap pair images. The utilized dataset is illustrated in Figure 3. We used 3077 images for training and 330 images for validation.

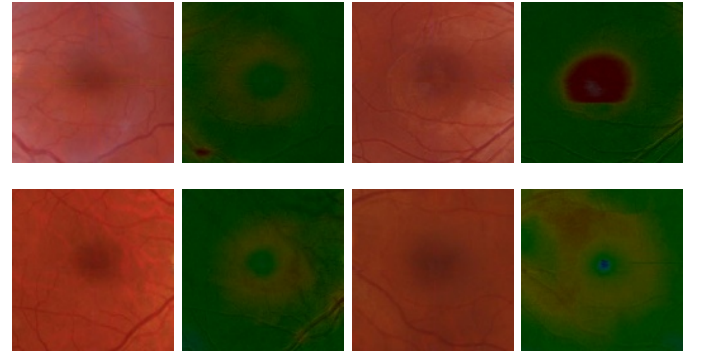


Fig. 3. Macula area on fundus image and their corresponding heightmap in our dataset.

### B. Experimental setup

We used Tensorflow 2.0 [23] for implementing our network. We also used Adam optimizer [24] with initial learning rate of  $1e^{-3}$  with a step decay of 0.9 per 30 steps. Moreover, we used the batch size of 8 and trained each experiment for 400 epochs to converge. Additionally, we set  $\lambda_1 = 5.0$ ,  $\lambda_2 = 1.0$ ,  $\lambda_3 = 5.0$  and  $\lambda_4 = 5.0$  in Equation 5 by trial-and-error and considering the contribution of each of them as discussed in [9], [11]. Finally, we updated the discriminator network after each three update to the generator network which resulted in more stable training.

### C. Evaluation metrics

In this work, we utilized a variety of different metrics to evaluate our final outcomes quantitatively. We measured the quality of the final image using the Structural Similarity Index (SSIM) [25], Mean Squared Error (MSE) and Peak Signal to Noise Ratio (PSNR). Nevertheless, these measures are insufficient for assessing structured outputs such as images, as they assume pixel-wise independence [15]. Consequently, we used Learned Perceptual Image Patch Similarity (LPIPS) [15] which can outperform other measures in terms of comparing the perceptual quality of images. We used features extracted from the  $1^{th}$ ,  $4^{th}$ ,  $6^{th}$  and  $8^{th}$  layer of the discriminator network to obtain the features and calculated the difference

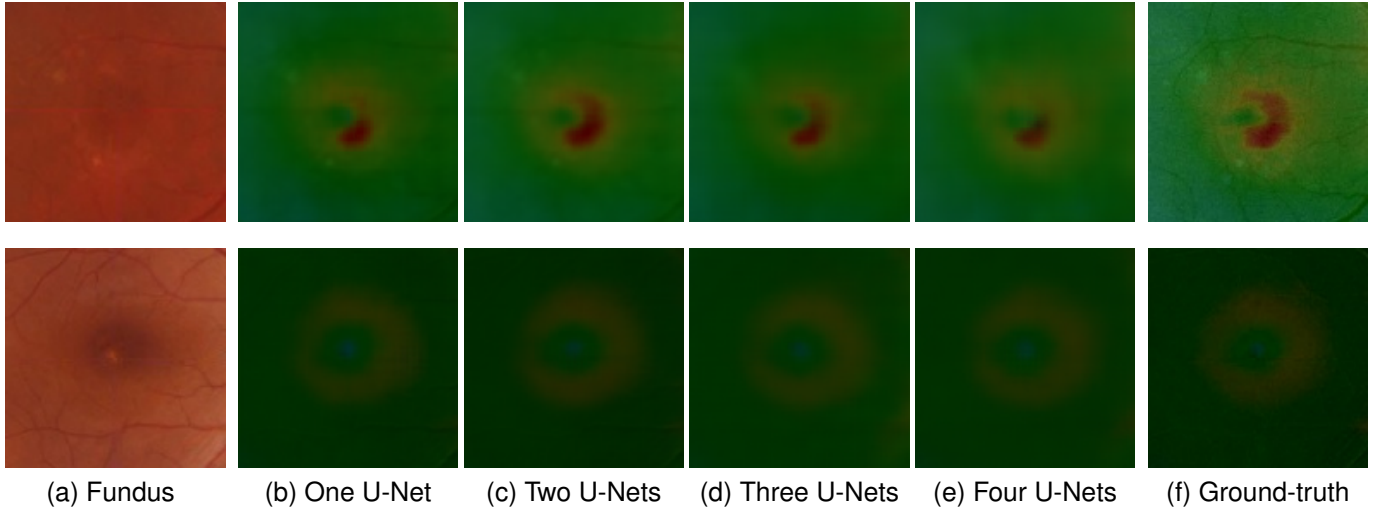


Fig. 4. Qualitative comparison in terms of different numbers of stacked U-Nets in generator structure.

between  $x$  as the generated heightmap and  $\hat{x}$  as the ground-truth heightmap using Equation below:

$$d(x, \hat{x}) = \sum_{l=0}^n \frac{1}{w_l h_l d_l} \| D_l(x) - D_l(\hat{x}) \|_2^2 \quad (7)$$

which all parameters are similar to Equation 4. For qualitative comparison, we present the ground-truth heightmap along with our generated heightmap.

#### D. Generator structure

In this part, we explore with different numbers of stacked U-Nets to find the optimum number. We set  $\alpha_1 = 100$ ,  $\alpha_2 = 1$  and  $\alpha_3 = 50$  in Equation 6 and used ImageGAN for our discriminator. The quantitative comparison is made in Table I. As can be seen, stacking two U-Nets resulted in higher values for SSIM and PSNR and lower values for MSE and LPIPS in comparison to one U-Net. However, the addition of more U-Nets deteriorated the results and, consequently, it seems that for this particular problem, stacking two U-Nets is the best possible option. Furthermore, qualitative comparison which is depicted in Figure 4 also supports our claim that two stacks of U-Nets is the best choice. As a matter of fact, the two U-Nets structure in this figure did well at predicting the full shape of the red region as well as the correct position and full shape of intense red spots. Additionally, it seems that by adding more U-Nets to the structure, the results become more blurry and details begin to vanish. Therefore, two U-Nets is the optimum number that preserves fine details and can produce plausible outcomes.

#### E. Discriminator structure

In this section, we seek to find the best choice for our discriminator network since a powerful discriminator is the key to successful training with GANs [5], [26]. We explored ImageGAN which measures the similarity of a given image to a ground-truth image and PatchGAN [8] which measures

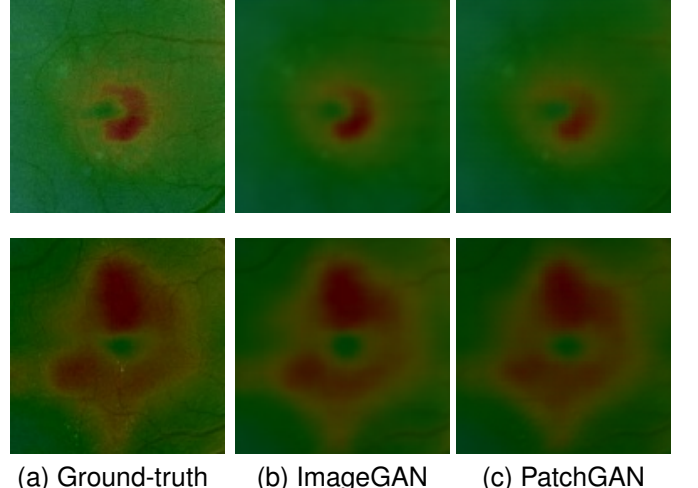


Fig. 5. Comparison between generated heightmap of PatchGAN and ImageGAN as the discriminator.

	SSIM	PSNR(dB)	MSE	LPIPS
1 U-Net	0.8843	34.8608	0.00062	2.77e-6
2 U-Net	<b>0.8953</b>	<b>35.7744</b>	<b>0.00048</b>	<b>2.73e-6</b>
3 U-Net	0.8549	32.6911	0.00099	4.90e-6
4 U-Net	0.8591	33.2958	0.00080	4.61e-6

TABLE I  
QUANTITATIVE COMPARISON BETWEEN THE DIFFERENT NUMBERS OF STACKED U-NETS IN GENERATOR STRUCTURE.

the similarity of a simple patch of the generated image to the ground-truth. For patchGAN, a 16x16 patch size was utilized by incorporating two convolutional layers with 64 and 128 spatial filters followed by batch normalization and Leaky-ReLU activation function. The ImageGAN structure is given in the third row of Figure 2. For a fair comparison, we also used perceptual loss for PatchGAN which extract features from both convolutional layers [6]. However, since we can only

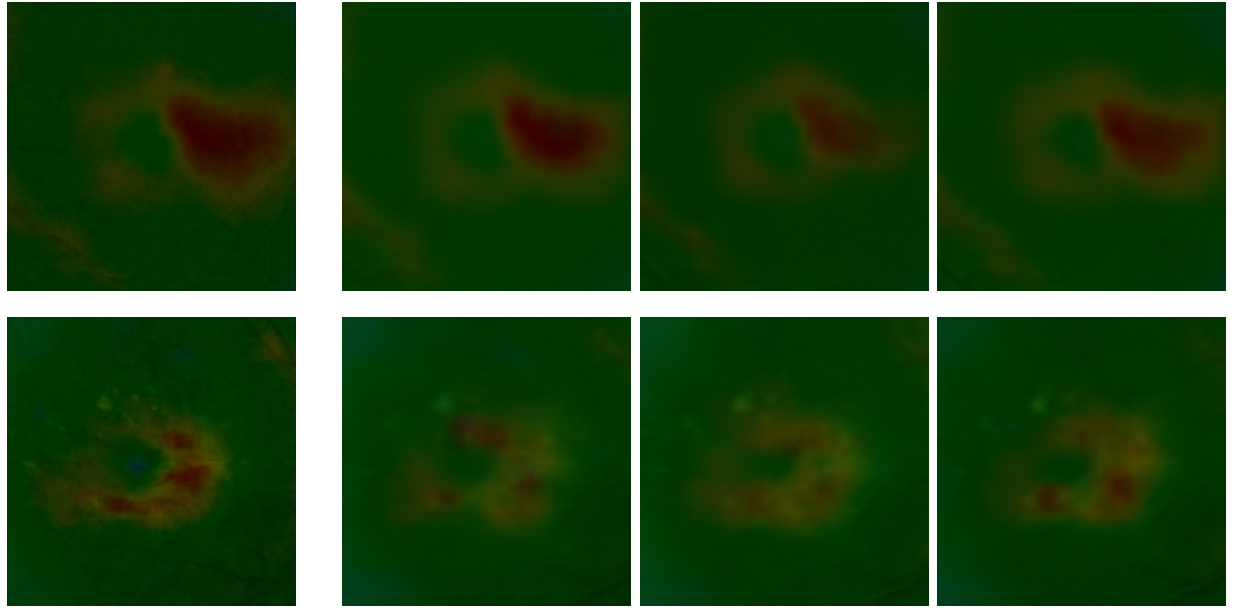


Fig. 6. Qualitative comparison considering the contribution of each of the objective functions.

utilize the output of two convolution layers for perceptual loss in comparison to four layers for ImageGAN, we opted to omit LPIPS which utilizes the output of the convolutional layer of the discriminator. The quantitative comparison between PatchGAN and ImageGAN is shown in Table II which clearly indicates the superiority of utilizing ImageGAN instead of PatchGAN. Additionally, the qualitative comparisons also

	SSIM	PSNR(dB)	MSE
PatchGAN	0.8659	35.0237	0.00052
ImageGAN	<b>0.8953</b>	<b>35.7744</b>	<b>0.00048</b>

TABLE II

QUANTITATIVE COMPARISON BETWEEN PATCHGAN AND IMAGEGAN.

support our claim that in this particular problem, the utilization of an ImageGAN is the better choice. As can be seen in Figure 5, in all examples, ImageGAN did better in terms of predicting intense red spots and correct shape of red regions.

#### F. Contributions of objective functions

In this section, we study the contribution of each of the three different objective functions used in this paper. First, we only used L2-Loss for image generation which yielded plausible results as can be seen in Figure 6b. To further refine our final output, we added GAN loss to study its contribution to the outcome. As can be seen in Table III, the addition of GAN loss to the L2-Loss improved the values which indicates its effectiveness in image generation tasks. In this experiment, we set  $\alpha_1 = 10$  and  $\alpha_2 = 1$  in Equation 6 by trial-and-error and to ensure that adversarial loss does not dominate the other losses [7]. Finally, we added perceptual loss to study its contribution with  $\alpha_3 = 50$ . As can be seen in Table III, perceptual loss

caused SSIM and PSNR to increase and MSE and LPIPS to decrease. In the case of LPIPS, it is obvious that the value will decrease since we are considering the difference between high-level features extracted from different convolution layers and trying to minimize it.

	SSIM	PSNR(dB)	MSE	LPIPS
L2	0.8820	34.6909	0.00051	3.74e-6
L2 + GAN	0.8935	35.7163	0.00049	2.82e-6
L2 + GAN + Perceptual	<b>0.8953</b>	<b>35.7744</b>	<b>0.00048</b>	<b>2.73e-6</b>

TABLE III  
QUANTITATIVE COMPARISON BETWEEN THE CONTRIBUTION OF EACH OF LOSS FUNCTIONS.

In addition to quantitative comparison, the qualitative comparison also indicates that the combination of three loss functions yields the best result. As can be seen in Figure 6d, the combination of three loss functions in both rows performed better at capturing the correct position of bright red spots.

#### G. L1-Loss vs L2-Loss

Even though in most of the papers L1-Loss is more common than L2-Loss as pixel-loss reconstruction loss [7], [8], [6], in this work we chose L2-Loss owing to emphasis that L2-Loss put on huge differences between generated image and ground-truth. As a matter of fact, since the difference in L2-Loss has a power of 2 like in Equation 3, small differences become minuscule and negligible and focus will be on huge differences. This behavior is perfectly suitable in this problem since our important goal is to predict regions that have a red color or blue color and it is acceptable to have inaccurate or blurry green areas or missed vessels. This is because those

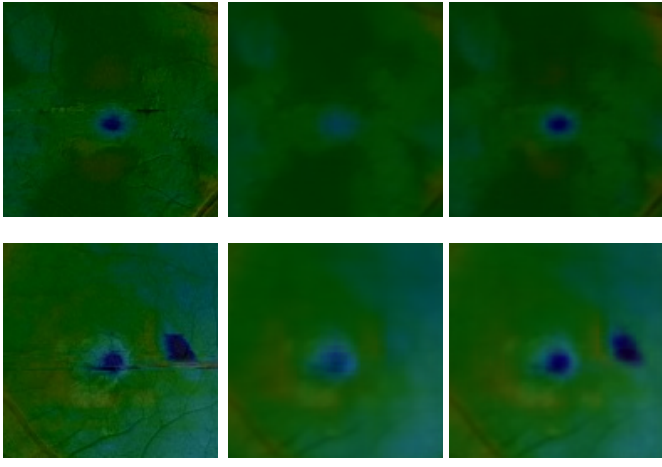


Fig. 7. Qualitative comparison between the output of L1-Loss and L2-Loss.

red regions or blue regions contain significant information for diagnosis. Our claim is supported by our experiment which we compared the results from L1-Loss and L2-Loss. Note that in this experiment the contribution of L2-Loss and L1-Loss function was equal along with GAN loss and perceptual loss. As can be seen in Table IV, L2-Loss performed better in all metrics and the difference is considerable. Furthermore,

	SSIM	PSNR	MSE	LPIPS
L1-Loss	0.8721	33.8351	0.00072	3.53e-6
L2-Loss	<b>0.8953</b>	<b>35.7744</b>	<b>0.00048</b>	<b>2.73e-6</b>

TABLE IV QUANTITATIVE COMPARISON BETWEEN L2-LOSS AND L1-LOSS.

regarding qualitative comparison in Figure 7, even though the global structure of images considering green areas is roughly the same, L2-Loss performed better at predicting blue regions which is crucial for diagnosis.

#### H. Comparison with Shape from Shading

In this section, we compare our output with the only method applied to this problem which utilized shape from shading [2]. For comparison, we used shape from shading using linear approximation method [27] to find the height of each of pixels in the scale of [0, 1] and then used a color bar like what we have in Figure 1 to generate a heatmap according to calculated height.

As can be seen in Table V, our method based on GANs outperformed the SFS method in all metrics. It is noteworthy that since in the SFS method we did not have any network layer to extract features from, we omitted the LPIPS in this experiment.

Considering qualitative comparison in Figure 8, in SFS method and in all illustrated examples, darker areas are assigned a more reddish color which means that it has more height. This is because in SFS, we consider the surface to have a normal and a gradient vector as well as a slant and tilt and

	SSIM	PSNR(dB)	MSE
SFS	0.2876	11.5568	0.0714
Proposed method	<b>0.8953</b>	<b>35.7744</b>	<b>0.0004</b>

TABLE V COMPARISON BETWEEN SFS AND THE PROPOSED METHOD IN TERMS OF SSIM, PSNR AND MSE.

it uses Lambertian assumption [13] which cannot be applied in retinal imaging. Additionally, this method only considers one pixel at a time and does not consider the relation between pixels nearby.

However, in neural networks and especially CNNs, we consider a patch of image for extracting features and pass it to the next layers. Therefore, it can detect the relation between different regions of the image and their impact on each other more easily to produce the output and, therefore, achieved the superior results in this problem.

## V. CONCLUSION AND DISCUSSION

In this paper, we proposed a framework to automatically generate a heatmap image of the macula on color fundus image. In this work, we used two stacked U-Nets for the generator along with ImageGAN for the discriminator. We also utilized traditional L2-Loss and GAN loss along with the perceptual loss to generate the final outcome. The experimental results indicate that our method outperformed the SFS method in terms of SSIM, PSNR and MSE metrics as can be seen in Table V. Furthermore, considering qualitative comparison in Figure 8, since our method utilizes CNNs and can capture the relation between pixels, it produces superior results in comparison to the SFS method.

However, our proposed method is not free from limitations and may fail in some cases. As can be seen in Figure 9, no useful information can be gathered from the generated heatmaps and the system failed to detect the red regions completely. One possible explanation for this is that in most failed cases, there were not sufficient information in fundus image to infer from and resulted in inaccurate generated heatmaps. Additionally, there are some rare cases in which the samples in our dataset for them is insufficient for learning and, therefore, adding more samples will improve our proposed method performance. Additionally, we expect that utilizing other features of fundus image besides automatic features extracted from CNNs can improve the overall performance of the proposed method. Finally, in future researches, we can utilize the results generated from our network to detect macular diseases from one fundus image and train more robust classifiers.

## REFERENCES

- [1] Peipei Wang, Fengliang Dai, Mengdie Zhao, Xiaojin Liu, and Jiuai Sun. Evaluation of retinal sfs reconstruction with oct images. pages 1–5, 10 2018.
- [2] Jini Cherian, B Hema, Hema Menon, and Narayanan Kuttu K.A. 3d reconstruction of human retina from a single fundus image. 04 2012.
- [3] David Huang, Swanson EA, Lin CP, Joel Schuman, Stinson WG, Chang W, Michael Hee, Flotte T, Gregory K, Puliafito CA, and Fujimoto JG. Optical coherence tomography. *Science*, 254:1178, 01 1991.
- [4] Fan Guo, Xin Zhao, Beiji Zou, and Pingbo Ouyang. 3d reconstruction and registration for retinal image pairs. pages 364–368, 06 2018.

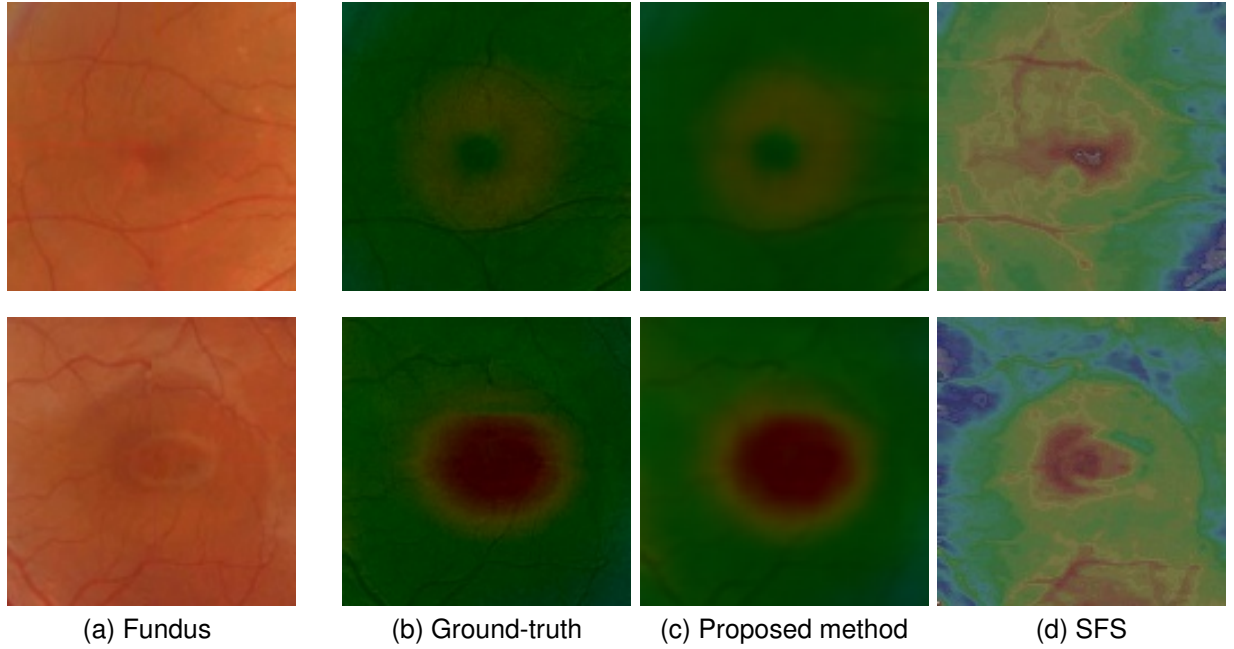


Fig. 8. Qualitative comparison between SFS and the proposed method.

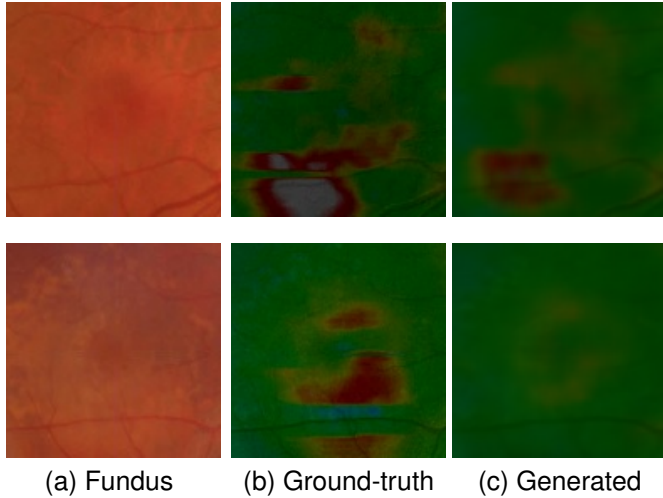


Fig. 9. Failed cases of the proposed method.

- [5] Ian Goodfellow, Jean Pouget-Abadie, Mehdi Mirza, Bing Xu, David Warde-Farley, Sherjil Ozair, Aaron Courville, and Y. Bengio. Generative adversarial networks. *Advances in Neural Information Processing Systems*, 3, 06 2014.
- [6] Karim Armanious, Chenming Yang, Marc Fischer, Thomas Küstner, Konstantin Nikolaou, Sergios Gatidis, and Bin Yang. Medgan: Medical image translation using gans. *Computerized medical imaging and graphics : the official journal of the Computerized Medical Imaging Society*, 79:101684, 2019.
- [7] He Zhang, Vishwanath Sindagi, and Vishal Patel. Image de-raining using a conditional generative adversarial network. *IEEE Transactions on Circuits and Systems for Video Technology*, PP, 01 2017.
- [8] Phillip Isola, Jun-Yan Zhu, Tinghui Zhou, and Alexei Efros. Image-to-image translation with conditional adversarial networks. pages 5967–5976, 07 2017.
- [9] Chaoyue Wang, Chang Xu, Chaohui Wang, and Dacheng Tao. Per-

- ceptual adversarial networks for image-to-image transformation. *IEEE Transactions on Image Processing*, PP, 06 2017.
- [10] Olaf Ronneberger, Philipp Fischer, and Thomas Brox. U-net: Convolutional networks for biomedical image segmentation. 05 2015.
- [11] Justin Johnson, Alexandre Alahi, and Li Fei-Fei. Perceptual losses for real-time style transfer and super-resolution. volume 9906, pages 694–711, 10 2016.
- [12] Richard Hartley and Andrew Zisserman. *Multiple View Geometry in Computer Vision*. Cambridge University Press, USA, 2 edition, 2003.
- [13] Ruo Zhang, Ping-Sing Tsai, James Cryer, and Mubarak Shah. Shape from shading: A survey. *IEEE Transactions on Pattern Analysis and Machine Intelligence*, 21:690–706, 08 1999.
- [14] Mehdi Mirza and Simon Osindero. Conditional generative adversarial nets. 11 2014.
- [15] Richard Zhang, Phillip Isola, Alexei Efros, Eli Shechtman, and Oliver Wang. The unreasonable effectiveness of deep features as a perceptual metric. 01 2018.
- [16] Christian Ledig, Lucas Theis, Ferenc Huszar, Jose Caballero, Andrew Cunningham, Alejandro Acosta, Andrew Aitken, Alykhan Tejani, Johannes Totz, Zehan Wang, and Wenzhe Shi. Photo-realistic single image super-resolution using a generative adversarial network, 2016.
- [17] Karen Simonyan and Andrew Zisserman. Very deep convolutional networks for large-scale image recognition. *arXiv 1409.1556*, 09 2014.
- [18] Jia Deng, Wei Dong, Richard Socher, Li-Jia Li, Kai Li, and Fei Fei Li. Imagenet: a large-scale hierarchical image database. pages 248–255, 06 2009.
- [19] Jianing Wang, Yiyuan Zhao, Jack Noble, and Benoit Dawant. *Conditional Generative Adversarial Networks for Metal Artifact Reduction in CT Images of the Ear*, volume 11070, pages 3–11. 09 2018.
- [20] Jaemin Son, Sang Jun Park, and Kyu-Hwan Jung. Retinal vessel segmentation in fundoscopic images with generative adversarial networks. 06 2017.
- [21] Talha Iqbal and Hazrat Ali. Generative adversarial network for medical images (mi-gan). 10 2018.
- [22] Kaiming He, Xiangyu Zhang, Shaoqing Ren, and Jian Sun. Deep residual learning for image recognition. pages 770–778, 06 2016.
- [23] Martin Abadi, Paul Barham, Jianmin Chen, Zhifeng Chen, Andy Davis, Jeffrey Dean, Matthieu Devin, Sanjay Ghemawat, Geoffrey Irving, Michael Isard, Manjunath Kudlur, Josh Levenberg, Rajat Monga, Sherry Moore, Derek Murray, Benoit Steiner, Paul Tucker, Vijay Vasudevan, Pete Warden, and Xiaoqiang Zhang. Tensorflow: A system for large-scale machine learning. 05 2016.

- [24] Diederik Kingma and Jimmy Ba. Adam: A method for stochastic optimization. *International Conference on Learning Representations*, 12 2014.
- [25] Zhou Wang, Alan Bovik, Hamid Sheikh, and Eero Simoncelli. Image quality assessment: From error visibility to structural similarity. *Image Processing, IEEE Transactions on*, 13:600 – 612, 05 2004.
- [26] Alec Radford, Luke Metz, and Soumith Chintala. Unsupervised representation learning with deep convolutional generative adversarial networks. 11 2015.
- [27] Ping-Sing Tsai and Mubarak Shah. Shape from shading using linear approximation. *Image Vis. Comput.*, 12:487–498, 1994.